ACS APPLIED ENGINEERING MATERIALS

pubs.acs.org/acsaenm Article

Programmable 4D-Printed Soft Actuators: Harnessing Bending Strain Distribution for Embedded Topological Functionality

Anas Saifi, Smruti Parimita, Amit Kumar, and Pijush Ghosh*

Cite This: https://doi.org/10.1021/acsaenm.5c00225 Read Online

ACCESS | Metrics & More | Article Recommendations | Supporting Information

ABSTRACT: Embedded programming plays a crucial role in 2D to 3D shape transformation by providing on-demand, precise, and localized control for applications ranging from soft robotics to biomedical devices. In this work, as a first of its kind, bending strain (or stress) distribution is applied on the TPU-BIFA composite to embed topology information in 2D, which transforms into a 3D structure with the corresponding topology when exposed to light. The internal bending strain distribution characteristics of the composite structure govern the poststimulant-triggered actuation or shape morphing. The internal strain distribution can be effectively varied through the magnitude and position of external loads and the boundary conditions. The prebending approaches of embedding topology are more useful for soft and planar structures with complex architecture. We also report an embedded composite ink 3D printing strategy to fabricate such complex structures by applying the principle of liquid−liquid phase separation. In addition to enabling programmability within the system, light as a stimulus offers great control over the actuators by tuning the light intensity and point of light irradiation. Upon irradiation with blue light (455 nm), the fabricated actuator performs well with omnidirectional light-triggered bending actuation of 20°/s and response rate of 60° in 8 s. As a proof of concept, phototunable curvature was demonstrated in complex architectures such as grids and human hand models by manipulating the prebending strain distribution. This work presents a comprehensive catalog of data generated by tuning various parameters to unveil a fresh horizon, which can be leveraged for programming complex geometries and opening avenues for smart polymers in biomimicry and biomedical applications.

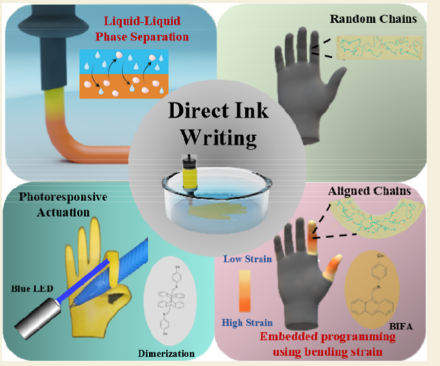

KEYWORDS: *embedded programming, bending strain, 4D printing, liquid−liquid phase separation, photoresponsive actuator*

1. INTRODUCTION

4D printing has emerged as an advanced manufacturing technique revolutionizing various sectors, including industry as well as research domain. Recently, Bodaghi along with the leading researchers across the globe provides a comprehensive review on the roadmap of 4D printing to guide the rapidly evolving field of 4D printing.[1] The key advantage of 4D printing over conventional 3D printing lies in the dynamic/adaptive behavior where the printed objects can change shape, function, or properties over time in response to external stimuli. Figure 1 shows the data generated using Scopus that illustrate the collaborative links between institutions and leading researchers actively publishing in the field of 4D printing.

Adaptive structures are ubiquitous in nature. The demand for replicating complex designs in nature using synthetic soft materials is ever-growing for various applications, such as soft robotics, biomimetics, drug delivery, dynamic substrates for tissue engineering, etc.[2−6] However, to fully harness the potential, these adaptive structures must be controlled and programmed at each point, defining the change in length and angle throughout the entire space.[7] Therefore, the objective of this work is to integrate the principles of mechanics into 4D-printed structures by embedding topological signatures to enable programmable actuation. A plethora of applications can benefit significantly from such precise control of the actuator. For instance, the human face has varied topography, including features like eyes, nose, and mouth, resulting in a variation in curvatures across the face. The transformation of a planar lattice into a 3D human face needs precise control.[7] The human hand endows us with unparalleled precision, where each finger can articulate in multiple ways and perform a wide range of tasks.[8,9] To illustrate further, the complexity of vascular networks varies greatly in shape within and across organisms.[10] The control over actuation may be crucial to developing dynamic scaffolds for these organs.[11] Such an independent control over the system is a challenging task to achieve experimentally.

Bending strain distribution is a critical concept of mechanics that refers to the variation of strain along and across the length of an element or structure when subjected to transverse load. The

Received: March 22, 2025
Revised: May 29, 2025
Accepted: May 30, 2025

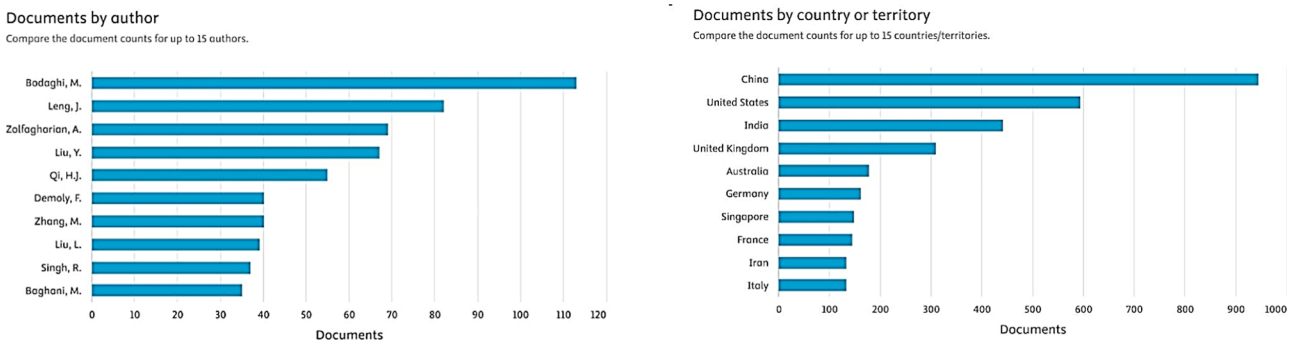

Figure 1. Global research network and leading researchers in 4D printing based on Scopus data.

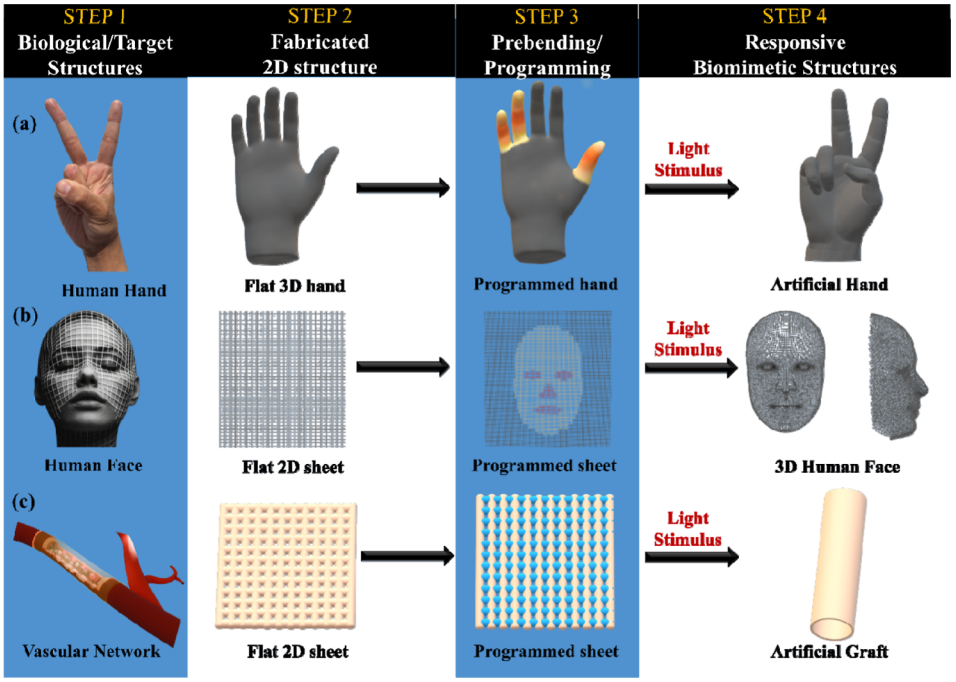

Figure 2. Schematically indicating the steps involved in designing and actuation of bending strain distribution on the embedded programmable actuator. Also, examples (a−c) show the potential applications.

corresponding stress distribution is called the bending stress distribution, which may be linearly or nonlinearly related to the former, depending on the materials involved. For embedding programmability in a soft actuator, the prebending strain distribution could provide an additional thrust by designing the distribution of strain throughout the structure. The traditional approach for programming photoresponsive soft actuators usually requires prestrain in the form of uniaxial stretching.[12,13] The uniaxial prestraining of the polymeric matrix aligns the coiled polymeric chains, bringing the photoresponsive moieties close to responding under the light stimulus.[14] However, when it comes to complex, planar soft structures with multiple joints or points of discontinuity, the uniaxial prestraining limits the adequate strain required in specific areas and thus limits only simple deformation. Therefore, the prebending strain distribution can be strategically and selectively controlled to achieve complex actuated shapes, as demonstrated in this work.

Furthermore, traditional manufacturing techniques often struggle to fabricate intricate 3D designs with soft materials.[15,16] The introduction of Direct Ink Writing (DIW), an extrusion-based 3D printing technique, enables precise, customizable fabrication of a wide range of soft materials, including liquid crystal elastomers,[17,18] hydrogels,[19−21] biological materials,[22−24] etc. However, they are often restricted to fabricating simple geometries due to the layer-by-layer deposition of viscoelastic material, which is susceptible to collapse. To address this limitation, several efforts have been made in the past for an immediate in situ curing mechanism to maintain the shape fidelity of the printed structures. For example, Hausladen et al. demonstrated a dual-core approach where UV-assisted photopolymerization followed by thermal curing of polyurethane elastomer was performed to improve the structural integrity,[25] Li et al. developed an in situ gelation method of cellulose nanofibrils hydrogel ink via ionic cross-linking. The addition of Ca-montmorillonite into cellulose nanofibrils improved the gelation strength.[26] However, these mechanisms still entail challenges, such as postprocessing, precise environmental conditions, additional material systems, equipment such as a UV light source, etc. Therefore, a simple, robust, and economic strategy is needed to showcase its potential in printing complex structures and reducing environmental footprints.

Liquid−liquid phase separation (LLPS) is a simple and faster method in which a polymer solution, when immersed in a

https://doi.org/10.1021/acsaenm.5c00225
ACS Appl. Eng. Mater. XXXX, XXX, XXX−XXX

nonsolvent, is separated into polymer-rich and polymer-lean phases, enabling immediate curing. The polymer-rich phase forms a structural matrix, while the polymer-poor phase helps form pores within the matrix.[27,28] Thermoplastic Polyurethane (TPU) has been of great interest to LLPS because of its simplicity, scalability, and shape memory behavior.[29−31] TPU is a widely used elastomer consisting of repeating soft and hard segments. Employing embedded 3D printing where TPU is printed inside a suspension bath can allow the printing of intricate 3D structures due to immediate curing and further broadens the ability to tune the complexity of the printed structure in response to a stimulus. TPU mainly responds to temperature when programming a temporary shape;[32] however, the temperature is not suitable for biomedical applications as it may harm the body tissues. Therefore, light can be an ideal stimulus, allowing localized, noncontact, and remote-controlled shape deformation.[33,34] Among various photoresponsive dyes, anthracene dye facilitates cross-linking by undergoing [4 + 4] cycloaddition reactions, thereby locking the temporary shape of the polymer.[35−37] However, using short-wavelength, high-energy UV light can potentially risk the body tissues and, therefore, is not recommended for biomedical applications.[38,39] In this work, a benzylamine-functionalized anthracene (BIFA) dye was prepared using Schiff base chemistry to demonstrate a visible-light-induced temporary shape fixation of TPU.[40]

In this contribution, we present an approach to designing complex architectures that can undergo localized and programmable actuation in response to light. We first demonstrate the embedded printing of a TPU-BIFA composite using the LLPS method, which leads to immediate curing. We further generated a data set by embedding programmability using bending strain distribution through the magnitude of load, position of load, and boundary condition. In addition to enabling programmability within the system, we demonstrated control over the actuator by varying the number of light irradiation points and the intensity of light. Thereafter, we designed a customizable photoresponsive deformation of grid structures and tuning of human finger curvature to demonstrate different tasks based on the knowledge of the data generated from the parameters mentioned above. The fabricated filaments exhibit outstanding performance with light-triggered bending actuation of 20°/s, response rate of 60° in 8 s, and mechanical properties (4.88 MPa). To the best of our knowledge, no previous literature has reported the printing of complex 3D structures, and their actuation based on programmable photoresponsive deformation using controlled prebending strain or stress distribution. We envisioned that this work provides a very robust approach to programming a soft actuator for biomimicry and personalized healthcare, where patient-specific demands can be fulfilled.

The concept of the bending strain distribution for programmable light-controlled deformation is schematically explained in Figure 2. Initially, the design of the actuator was inspired by various biological structures, which served as motivation for replication (step 1). These are also the target structures based on intended applications. The next step involves designing the basic 2D structure using the DIW 3D printing technique (step 2). Once the 2D structure is printed, the next step is to program the structure by embedding the topology of the desired shape (step 3). This step predetermines how the actuator will behave in response to light as a stimulus. The programming is performed using the strain distribution throughout the structure by applying load to specific areas. Finally, in step 4, the programmed structure is exposed to light to transform from a simple 2D structure to the desired 3D topology for which it was programmed in step 3.

Programming a 2D structure is not limited to specific shapes but can be easily morphed into various shapes for diverse applications. This flexibility in embedding topology by bending strain distribution opens up a new avenue, enabling the design of smart actuators that can be tuned for specific functionalities for various applications, from soft robotics to biomedical applications, and even for designing deployable structures for space applications.

2. EXPERIMENTAL SECTION

2.1. Materials

Thermoplastic Polyurethane granules with shore hardness 92A (LARIPUR LPR 9020) were purchased from Anoopam India Pvt. Ltd. 9-Anthracenecarboxaldehyde and 4-aminophenol were purchased from TCI Chemicals. Acetic Acid glacial was procured from Sigma. Dimethylformamide and methanol were purchased from SRL Pvt. Ltd. Deionized water was obtained from the equipment Aquelix 5 Millipore. All of the reagents were used without further purification.

2.2. Fabrication Process

2.2.1. Synthesis of Benzylimine-Functionalized Anthracene Dye. A benzylimine-functionalized anthracene dye (BIFA) was prepared, as reported previously.[39] Briefly, 100 mL of anthracene precursor dye (1.6 g) was prepared in a mixture of Methanol:DMF (8:2, v/v). To obtain a homogeneous solution, the mixture was refluxed at 60 °C, followed by the addition of 4-aminophenol solution (872 mg in 20 mL of methanol). The orange crystals precipitated after adding ice acetic acid, and the mixture was refluxed for another 8 h. The orange crystals were filtered, washed with D.I. water, and dried at 50 °C for further use.

2.2.2. Embedded 3D Printing of a TPU-BIFA Composite Ink. Initially, TPU granules (20 g, 40 wt %) were added to DMF (50 mL) and mixed using a mechanical stirrer (300 rpm) at 90 °C until a homogeneous solution was prepared. Meanwhile, BIFA solutions of different concentrations (1, 2, and 5 wt % of TPU) were prepared in DMF and added dropwise to the TPU solution under constant stirring at 60 °C. Afterward, the obtained homogeneous composite ink was transferred to the syringe for further use.

The prepared TPU-BIFA composite ink was extruded in water by using a custom-built DIW 3D printer. STL models were generated using SolidWorks and imported into Ultimaker Cura for slicing files. The printing process involved loading a syringe (50 mL) with composite ink, then using a 1 bar pressure on a nozzle (19G) to print at a speed of 5 mm s^{-1}. Due to the phase separation process, the composite ink solidifies immediately after extrusion into water. The printed structures were left in water for 30 min to complete the phase separation process and then dried overnight at room temperature.

2.3. Characterization

The rheological behavior of pure TPU and the TPU-BIFA composite was investigated using a rotational rheometer (MCR301, Anton Paar, Austria). The samples were placed using a 25 mm parallel plate with a measurement gap of 1 mm. The viscosity of the printable ink was measured at room temperature with shear rates ranging from 0.1 to 1000 s^{-1}. Attenuated Total Reflectance Fourier Transform Infrared (ATR-FTIR) was performed using a TENSOR II FTIR Spectrophotometer from Bruker Optics over a range of 400−4000 cm^{-1} with a resolution of 8 cm^{-1} and 64 scans were performed to analyze the chemical structures of the samples. The UV−vis absorption measurements were carried out with a Cary 4000 UV−vis double beam spectrophotometer. The alignment of the fabricated samples was then analyzed using X-ray diffraction (XRD) spectrometry (X'Pert3 Powder, Malvern PANalytical, UK) in the range of 4°−70° with a time step of 0.6 s. The mechanical properties of the samples were characterized by a universal tensile testing machine (1ST Tinius Olsen); the machine was equipped with a 1 kN load cell, and the stretchability of the filaments (40 mm gauge length) was measured at a speed rate of 15 mm min^{-1}.

https://doi.org/10.1021/acsaenm.5c00225
ACS Appl. Eng. Mater. XXXX, XXX, XXX−XXX

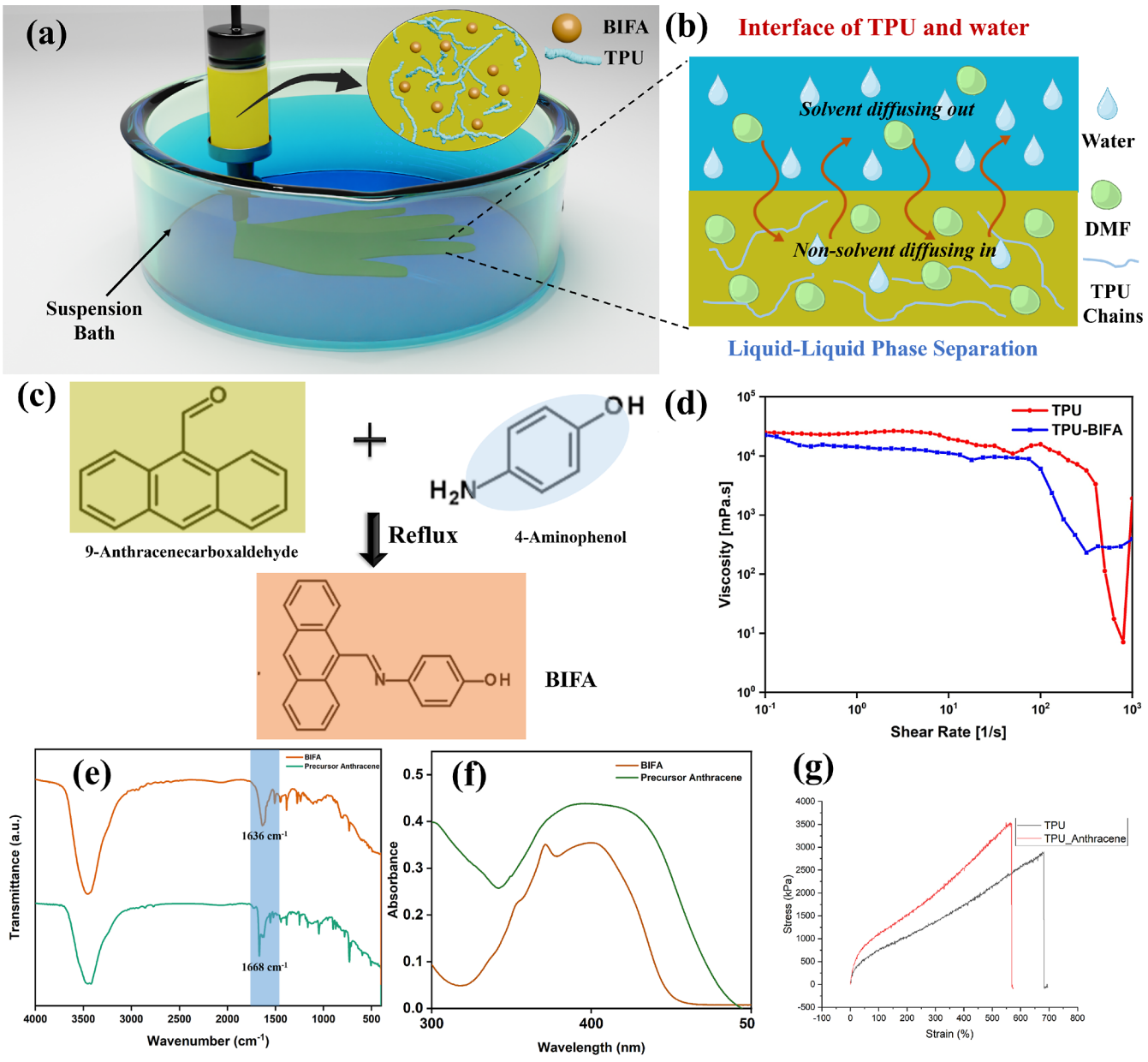

Figure 3. (a) Schematic illustration of embedded ink 3D printing of a human hand using a liquid−liquid phase separation mechanism. (b) An enlarged image of TPU and water interface, displaying the exchange of water and DMF, leading to immediate curing of TPU. (c) Molecular design of BIFA synthesis using Schiff base chemistry. (d) Rheological characterization of 40 wt % TPU and TPU-BIFA composite printable ink. (e) FTIR spectra of precursor anthracene and BIFA dye. (f) UV−vis spectra for monitoring the conjugation of precursor anthracene to synthesize BIFA dye. (g) Stress−Strain curve of 40 wt % TPU-BIFA (15 mm min^{-1}).

Thermogravimetry investigations of TPU and its composite ink were conducted using a Q500 Hi-Res TGA (TA Instruments, Inc.). Samples were heated in nitrogen or air atmospheres at a heating rate of 10 K/min. The morphology of the cross-sectional filament was obtained by high-resolution scanning electron microscopy (HR SEM) (S-4800, Hitachi(R)) under an accelerating voltage of 1−3 kV. The blue LED light (455 nm, 190 mW cm^{-2}) and LED driver were purchased from Holmarc Opto-Mechatronics Ltd., Kochi, India, to study the light-responsive actuation. The temperature changes on the surface of the irradiated filaments were measured through a thermal infrared imager (FLIR). The actuation of the samples was analyzed by using ImageJ software. A cantilever-based blocked force measurement setup was used to measure the force generated by the filaments.

3. RESULTS AND DISCUSSION

3.1. Embedded Ink 3D Printing of Complex Structures

This work aims to utilize bending strain distribution within the 3D printed structures to generate complex shapes when they are exposed to light stimuli. Before going to programming and actuation, the embedded ink writing 3D printing technique was employed for the printing of 3D intricate structures inside a suspension bath. The mechanism of embedded ink 3D printing of a TPU-BIFA composite is schematically illustrated in Figure 3a. The composite ink was printed by using a liquid−liquid phase separation (LLPS) method. Initially, the printing ink was prepared by homogeneously mixing BIFA dye into a TPU solution to impart photoresponsive behavior. The ink was introduced into the syringe and extruded with a nozzle (size

https://doi.org/10.1021/acsaenm.5c00225
ACS Appl. Eng. Mater. XXXX, XXX, XXX−XXX

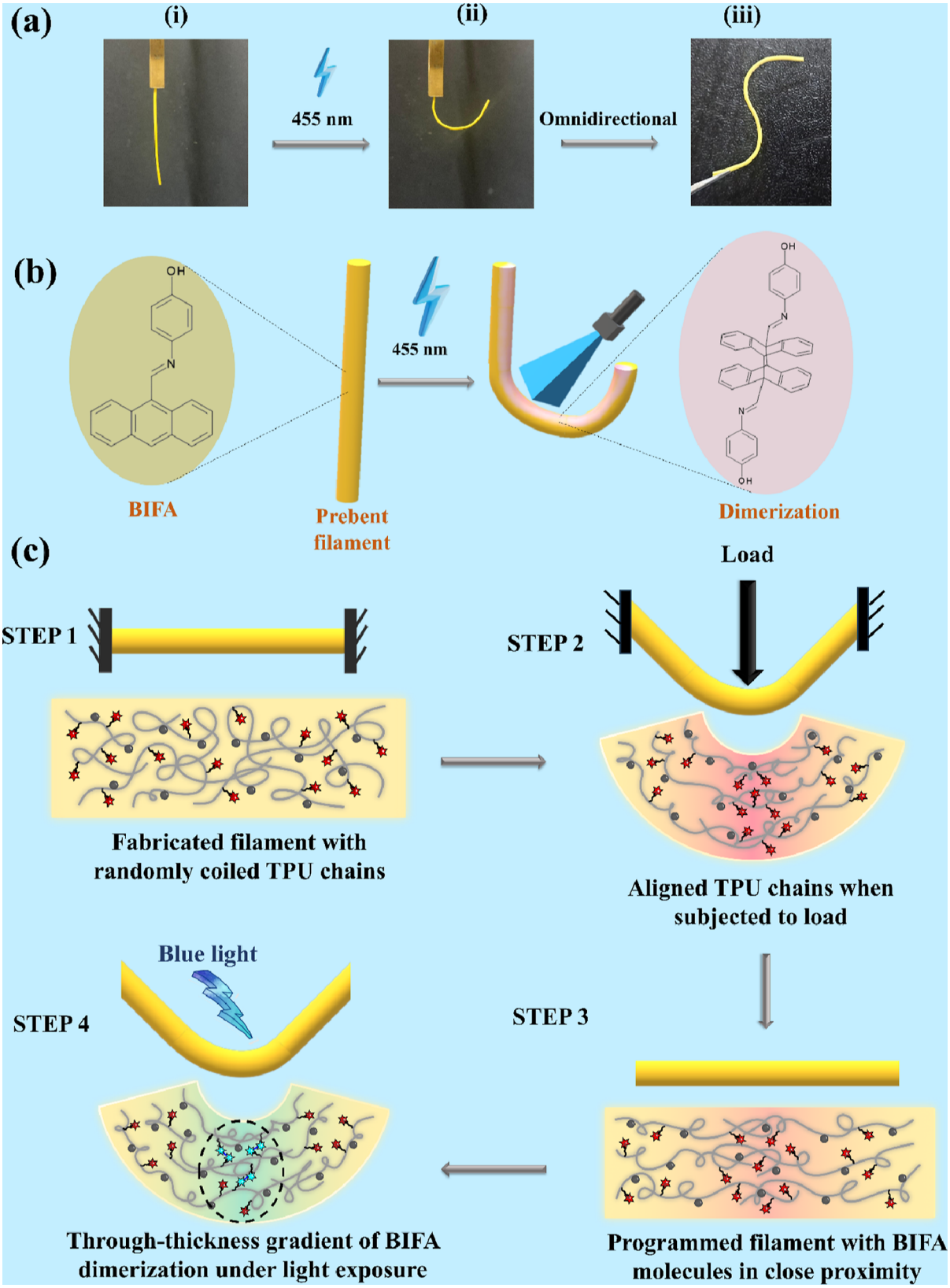

Figure 4. (a) Photomechanical deformation of a TPU-BIFA filament in response to blue light (i) before prebending strain, (ii) after prebending strain, (iii) omnidirectional movement by changing the direction of the light irradiation. (b) Schematic illustration of the light-induced actuation due to a through-thickness gradient formed by the photodimerization of BIFA dye in a prebent filament. (c) Schematic illustration of the steps involved in programming and chain alignment of the filament using bending strain.

19G) with 1 bar of pressure. Water was chosen as a suspension bath for embedded printing because it is a nonsolvent for TPU (dissolved in DMF). DMF acts as a good solvent for TPU, where the polymeric chains are uniformly dispersed. When extruded in

https://doi.org/10.1021/acsaenm.5c00225
ACS Appl. Eng. Mater. XXXX, XXX, XXX−XXX

water, the ink undergoes phase separation because water molecules gradually diffuse into the polymer and disrupt the solubility of TPU. TPU polymer chains start aggregating into a polymer-rich domain and immediately solidify, leaving water inside the polymer-lean domain (Figure 3b).[28] After drying the printed structure in the air, water gradually evaporated, and the interconnected porous structure of TPU-BIFA was formed, as shown in the SEM images (Figure S1). A video of the printing process of a grid structure can be found in the Supporting Information, Video S1.

For successfully printing viscoelastic materials, the rheological characteristics of the ink play an important role in determining the shape fidelity of the final structure and eventually the actuation rate. The steady-state shear test was performed at room temperature to investigate the extrudability of the composite ink (Figure 3d). When the shear rate is increased, the viscosity of the ink decreases, attributing to the ink's shear thinning property and ensuring the ink's smooth extrudability without clogging the nozzle.[19] It was observed that there was a slight decrease in the viscosity of TPU after introducing BIFA dye, which increases the polymer chain mobility.

The molecular design of printing ink, composed of a functionalized anthracene moiety, was characterized by FTIR. Figure 3c shows the molecular schematic of the synthesis of visible-light-responsive BIFA dye using Schiff base chemistry, where an imine bond was introduced to increase the conjugation. The characteristic peak at 1636 cm^{-1} confirmed the presence of an imine functionality, as shown in Figure 3e. UV−vis spectroscopy was conducted to determine the increased conjugation in BIFA for the visible light response, exhibiting a strong absorbance peak in the 400−460 nm region, which was distinguished from the typical UV light-responsive precursor anthracene (Figure 3f). To determine the mechanical properties, the TPU-BIFA filament (40 mm gauge length) was extruded from a 19G nozzle to perform the tensile testing. The tensile strength of the 3D-printed TPU (3.19 MPa) was improved after the addition of BIFA to TPU (4.88 MPa), which is attributed to the fact that BIFA acts as a filler and improves the mechanical properties (Figure 3g). The thermal properties of TPU further improved after the inclusion of BIFA. The decomposition of TPU occurs in two stages due to the presence of hard and soft segments. Figure S2 shows that the initial thermal stability of TPU is increased following the introduction of the BIFA dye.

After the successful printing of the structures using the LLPS technique, the fabricated structures were subjected to bending strain, enabling the embedded programmability within the structure. This aspect of the bending strain distribution is discussed in detail in the following section.

3.2. Bending Strain for Localized and Programmable Photoresponsive Actuation

Initially, we exposed the filament made of the TPU-BIFA composite to blue light; however, no macroscopic deformation was exhibited, as shown in Figure 4a(i). This could be attributed to the fact that initially, it contains coiled polymeric chains, and BIFA molecules are embedded in positions where dimerization is not possible when exposed to blue light.[14,41] However, after we applied a bending strain to this filament and exposed it to blue light, it morphs in the direction of light, as shown in Figure 4a(ii). The applied bending strain helped align the polymeric chains of TPU and bring the photoresponsive moieties close to each other, resulting in photomechanical deformation when exposed to blue LED light. We used solid tubular filaments that can bend in any direction depending on the direction of the irradiation of light. Figure 4a(iii) and Video S3 show the formation of the "S" shape by irradiating the light from the top and bottom sides, exhibiting omnidirectional movement.

The deformation of TPU-BIFA filaments results from the photodimerization of BIFA moieties within the aligned polymeric chains of the TPU matrix. The fabricated filaments formed by applying the phase separation principle were typically opaque. Due to its inherent opacity, light penetration depth is limited, and thus, dimers cannot be formed uniformly across the thickness. This leads to a through-thickness gradient in cross-linking density, which contributes to the macroscopic deformation (Figure 4b).[42] Since light can be localized in time and space, the cycloaddition reaction induced by light may result in local cross-linking of the actuator. When light is applied to a specific portion of the filament experiencing bending strain, the local cross-linking density pulls the polymeric chains closer, thus bending toward the light. After the actuation strain reaches the plateau, the light is moved to another point, and the same reaction occurs, potentially leading to cross-linking in the new area. Consequently, a more pronounced bending angle was observed, as shown in Video S2.

In earlier works, researchers applied uniaxial prestraining to align the polymeric chains in the direction of the applied force. This approach has significant limitations since it can be applied to extremely simple structures and uniform deformation. For generating complex shapes, the out-of-plane bending strain can be useful for embedding programmability, as it provides localized control over the chain alignment at each point of the actuator. Before demonstrating the deformation of a complex structure with the programmed distribution of bending strain, we illustrate the concept of obtaining different deformations through a simple strand filament. Figure 4c shows the steps involved in the embedded programmability (step 1), a 3D-printed filament with randomly coiled polymeric chains where BIFA molecules are distributed in areas where it is challenging to form dimers. In step 2, when the filament is subjected to load developing bending strain, the polymeric chains align themselves (according to the stress−strain distribution), bringing the BIFA molecules into close proximity. The position of the load results in the local concentration of BIFA molecules due to the alignment of the polymeric chains in the region of the subjected load. Step 3 shows the relaxed filament (with some residual strain) after removal of the load. In Step 4, when irradiated with light, more dimers form in the area with a higher magnitude of bending strain than in the other regions with a lower magnitude of strain. This is the most important design aspect of the proposed work, where the bending strain/stress distribution (magnitude and position) determines the actuation curvature. Additionally, due to through thickness gradient, the top (exposed) region of the filament forms more dimers than the bottom part of the filament to achieve the desired actuation. This strategy may also help in tuning the curvature of the actuator, in addition to the strain distribution. The change in the molecular chain alignment by prestrain was studied using XRD (Figure S3). The TPU-BIFA has a broad peak around $2\theta = 20°$, suggesting an amorphous TPU filament. The XRD pattern of TPU-BIFA with prebending strain reveals a sharp peak with increased intensity, attributing to an orderly arrangement of TPU molecular chains corresponding to the recrystallization of the soft domain.[41]

https://doi.org/10.1021/acsaenm.5c00225
ACS Appl. Eng. Mater. XXXX, XXX, XXX−XXX

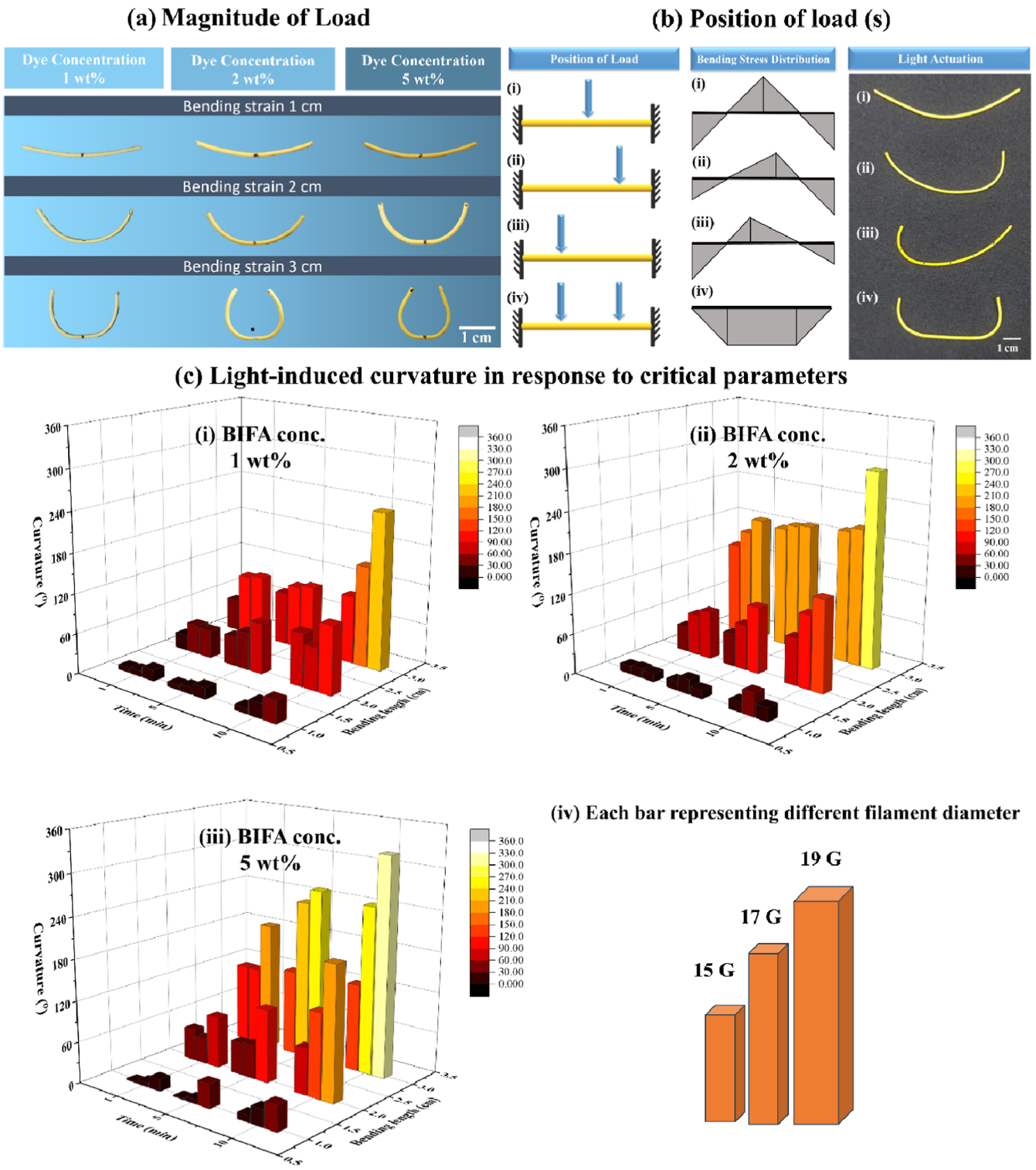

Figure 5. (a) The final curvatures of filaments of different BIFA concentrations by varying the bending strain for 10 min. (b) Schematic illustration of bending stress distribution and their corresponding photomechanical deformation of the different positions of the subjected load on the filament. (c) The relationship between light-induced curvature for different concentrations of BIFA dye (i) B1, (ii) B2, (iii) B and the critical parameters (bending strain, duration of bending strain, filament diameter). (iv) Each point has 3 bar representing different diameters, i.e., 15 to 19 G from left to right.

The photoresponsive behavior of the BIFA dye was also investigated at the molecular scale. UV−vis spectroscopy was used to detect the absorbance characteristics where a strong absorbance was observed in the visible region (400−460 nm) due to the $\pi-\pi^*$ transition. After exposure to blue light (455 nm), absorbance decreased because the conjugated system was broken to form dimers with the neighboring anthracene groups (Figure S4).[43,44] These results suggest that the synthesized BIFA dye is responsive to blue light.

The light-induced changes in the surface temperature of the filament were measured by using an infrared camera (Figure S5). In the photothermal images, no significant changes were

https://doi.org/10.1021/acsaenm.5c00225
ACS Appl. Eng. Mater. XXXX, XXX, XXX−XXX

observed upon variation of the light intensities. For example, under the low light intensity (28 mW cm^{-2}), the surface temperature was about 38 °C, whereas the maximum temperature attained with maximum intensity of light (190 mW cm^{-2}) was 49 °C. These results suggest that the actuation of the filament does not correspond to the photothermal effect but rather is mainly due to the photodimerization effect of BIFA molecules.[45]

3.3. Shape Programming with Varying Strain Distribution

Light actuation and bending strain enabled us to delve further into studying the localized manipulation and programming of the filament curvature. Understanding the relationship between transverse load and the actuation curvature is crucial for precise control, ensuring the customization of an actuator based on the individual's needs. Our goal was to prepare a catalog of tunable curvature by programming through various parameters, such as magnitude and position of load, stiffness of the filament, and light irradiation conditions. The reported curvatures are solely determined from the actuation, with the residual curvature, if any, due to the viscoelastic nature of TPU, subtracted from it. For ease of explanation, the following parameters were denoted as filament length (L1 and L2 for 3 and 6 cm), BIFA conc. (C1, C2, and C3 for 1, 2, and 5 wt % of TPU), bending strain (S1, S2, and S3 for 33%, 66%, and 100%), and duration of load applied (T1, T2, and T3 for 1, 5, and 10 min).

3.3.1. Magnitude of Load. Initially, the light-induced curvature of the TPU-BIFA filament was investigated by varying the internal bending strain/stress distribution through an externally applied load of (a) different magnitudes and (b) durations of application (Figure 5). The filament (L1) was subjected to point load at the center by varying three different magnitudes of bending strains, i.e., 33%, 66%, and 100%. After the load was applied, the filaments were relaxed from the fixed ends. Then, they were subjected to light irradiation. For the same position of a load, an increase in the magnitude of bending strain exhibited increased light-induced curvature.[46] The filaments with a bending strain of 33% exhibited a bending angle of 30°, which can be attributed to fewer TPU chains being aligned, limiting the number of photoresponsive moieties to form photodimers. However, increasing the bending strain to 66% and 100% increases the internal strain and allows more TPU chains to align, bringing the photoresponsive moieties close enough to form photo dimers, leading to a greater curvature. The above observations, in particular, demonstrate the effect of the bending strain distribution across depth/thickness on the curvature. Most of the examples in the following section, however, focus on the effect of strain distribution along the length on the attained curvature. It is important to notice that the curvature of the filament can also be controlled by the duration of the applied load on the element, as shown in Figure 5c. This is because TPU, together with photoresponsive moieties, undergoes creep. We, however, at present, have not understood the nature of the creep (primary, secondary, or tertiary) responsible for the effect of duration of loading on actuation. When the constant load was subjected for time T1, the curvature varied as 17°, 38°, and 188° for the bending strains of S1, S2, and S3, respectively. As the duration of subjected load increases, the internal creep causes the light-induced curvature to exhibit an increasing trend of 35°, 107°, and 255° for S1, S2, and S3 at T2 and 38°, 196°, and 322° for S1, S2, and S3 at T3, respectively. The influence of the BIFA dye concentration on the light-induced curvature of the filament was also investigated. When the duration of the applied load is kept constant, the curvature of the filament varied as 236°, 294°, and 322° for BIFA concentrations of C1, C2, and C3, respectively. The higher dye content leads to a higher degree of photo-cross-linking and a greater curvature.[35] These results confirm that the magnitude and duration of the bending strain significantly influence the light-induced curvature of the printed filaments.

3.3.2. Position of Load. The position of the subjected load is another crucial parameter to achieve different internal strain distributions and, thus, the final curvature of the filament, as demonstrated in Figure 5b. When the load is applied at different positions, it creates a varying stress distribution within the filament, leading to programmable deformation of the filament. We studied the actuation by changing the position of the transverse loads. When the external load was placed at the center, the stress distribution was symmetric; therefore, a uniform bending was observed. However, the stress distribution and, thus, the internal strain distribution was asymmetric when the transverse load was applied away from the center, resulting in more pronounced actuation toward the side where the load was applied. It was interesting to note that the actuation profile can be further modified by subjecting filaments to multiple loadings, since the latter alters the internal bending strain distribution differently.

Later, the impact of combining two loads at different positions of the filament was investigated. As shown in Figure S6, the filament was divided into ten segments (0.6 cm each), and the two-point loads (symmetric and asymmetric) were subjected to different points on each side from the center to observe the curvature at every point when exposed to light. Compared with the single load, a more complex deformation was obtained with two-point loads.

3.3.2.1. Load Symmetry/Asymmetry. For symmetric loading, the filaments were subjected to two-point loads at equal distances from the center. The resulting filaments exhibited a uniform curvature between the loads when exposed to light. This matches the pattern of the stress distribution shown on the left. To monitor the changes more intuitively due to varying bending stress distribution, the two loads were unevenly distributed along the filament. When exposed to light, it exhibited a more complex curvature, where stress-concentrated regions displayed a sharp curvature upon light irradiation compared to the other parts of the filament. When we look around us, we find that asymmetric curvatures are often more prevalent compared with symmetric curvatures. Therefore, this study may help mimic the asymmetric structures for better adaptation to natural or practical applications. The illustration presented above laid the foundation for programming the actuation profile of the filament based on internal strain distribution via regulating the position of the transverse load(s). It is realized that although bending stress is a nonlinear function of bending strain for materials of this kind, one is a monotonically increasing function of the other. This is the reason we are synonymously using stress and strain distribution.

3.3.3. Filament Stiffness. Stiffness is another crucial parameter in determining bending strain distribution, as it influences how a material deforms under the applied load. We studied the influence of the stiffness on the light-induced curvature by varying the filament diameter using different nozzle diameters (15, 17, and 19 G). Increasing the filament's diameter results in a decrease in curvature on light actuation due to increased stiffness (Figure 5c).[46] Additionally, the light penetration depth may also partially contribute to the actuation

https://doi.org/10.1021/acsaenm.5c00225
ACS Appl. Eng. Mater. XXXX, XXX, XXX−XXX

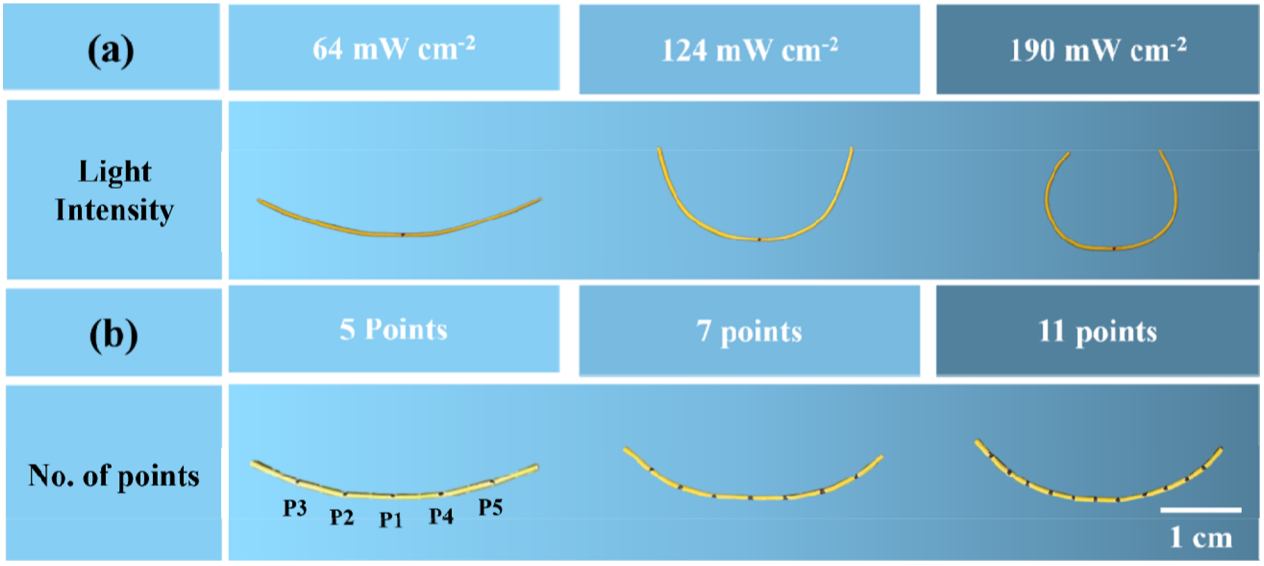

Figure 6. Light-induced curvature of the B5 filament (a) with varied light intensities (64, 124, and 190 mW cm^{-2}), (b) with varied light irradiation points (5, 7, and 11 points).

process. In opaque filaments, light can only penetrate up to a certain distance; i.e., light penetration depth decreases with increasing filament thickness. This coupled effect of penetration depth should be taken into account while designing the filament diameter for the desired curvature. These results suggest that stiffness (structure dimension) can also be tuned to attain a final curvature.

Besides bending strain distribution, we also studied how light can affect the actuation characteristics of the fabricated filaments. Due to spatiotemporal control, light can be easily localized to a specific portion of the filament, and its intensity can also be tuned to change the actuation profile.

3.3.4. Effect of Light Intensity. The intensity of the light is another parameter that can also play a crucial role in tuning the curvature. The photomechanical response of the TPU-BIFA filament was studied with different intensities (64−190 mW cm^{-2}) of blue light. The results demonstrated that the curvature of the filament improved gradually with an increase in the intensity of blue light (Figure 6a). This could be ascribed to the formation of a higher number of dimers compared to filaments irradiated with lower-intensity light. When the intensity increased from 64 to 190 mW cm^{-2}, the bending curvature improved from 60° to 322°.[46]

3.3.5. Position of Light Irradiation. Light offers unique precision and spatiotemporal control over the actuator. Instead of completely scanning the filament with light, we can selectively irradiate the filament in a discrete fashion to achieve the required deformation. Here, we investigated the effect on the curvature by changing the number of light irradiation points on the filament for the same bending strain distribution. The length of the filament was kept constant (6 cm), and we changed the number of light irradiation points, i.e., P1 = 5, P2 = 7, and P3 = 11 (Figure 6b). As the number of light irradiation points increased, the curvature of the filament started increasing from 56°, 96°, and 120° for P1, P2, and P3, respectively. This results from the local cross-linking of BIFA moieties at each point, resulting in a more pronounced curvature with increasing light irradiation points. Another way of explaining it is the cumulative effect of strain at more than one point on the curvature. The change in curvature after selectively irradiating every point of the filament is shown in Figure S7.

The parametric studies performed above have demonstrated how the bending strain distribution can influence the bending angle of the fabricated filament on exposure to light. These insights will play an instrumental role in providing a fundamental understanding of the development of more complex structures, as demonstrated in the following section.

3.4. Controlled Deformation of 4D Printed Construct

The fundamental concept of embedded programming using prebending strain and light irradiation conditions is explained above. Numerous applications can be envisioned applying this concept with a transformative potential in robotics, actuators, tissue engineering, sensors, etc., as highlighted by Bodaghi and team in their recent article outlining the roadmap for 4D printing.[1] The advent of smart materials and additive manufacturing has open up avenues for new age soft robotics.[47] In this work, we designed and developed two 3D-printed structures (i) grid-like and (ii) human hand-like structures for light-controlled deformation. These designs hold significant potential in the field of biomedical engineering, particularly for customizable vascular grafts and scaffolds and soft robotic hands for surgical manipulation.

3.4.1. Soft Grids. The quest for complex structures that can attain different shapes is ubiquitous, especially in biomedical applications. Afzali Naniz et al. presented a comprehensive overview of the potential of 4D bioprinting in tissue regeneration, further emphasizing on how harmless stimulus like light could benefit to remotely control the shape transformation of the printed organ.[48] Figure 7a shows the schematic representation of the steps to program a plane 2D grid structure to attain the shape of an artificial vascular graft. In this work, two types of grid constructs were printed, i.e., one-grid (3 × 3 cm) and two-grid (6 × 3 cm) constructs, that can be programmed for a desired shape in response to blue light. In Figure 7b, the one-grid construct was subjected to load on the center of all four sides. This leads to symmetrical (approximately) bending strain distribution for each side, with the maximum being at the center. When irradiated with light, it deforms into a flower-like structure with curved edges,

https://doi.org/10.1021/acsaenm.5c00225
ACS Appl. Eng. Mater. XXXX, XXX, XXX−XXX

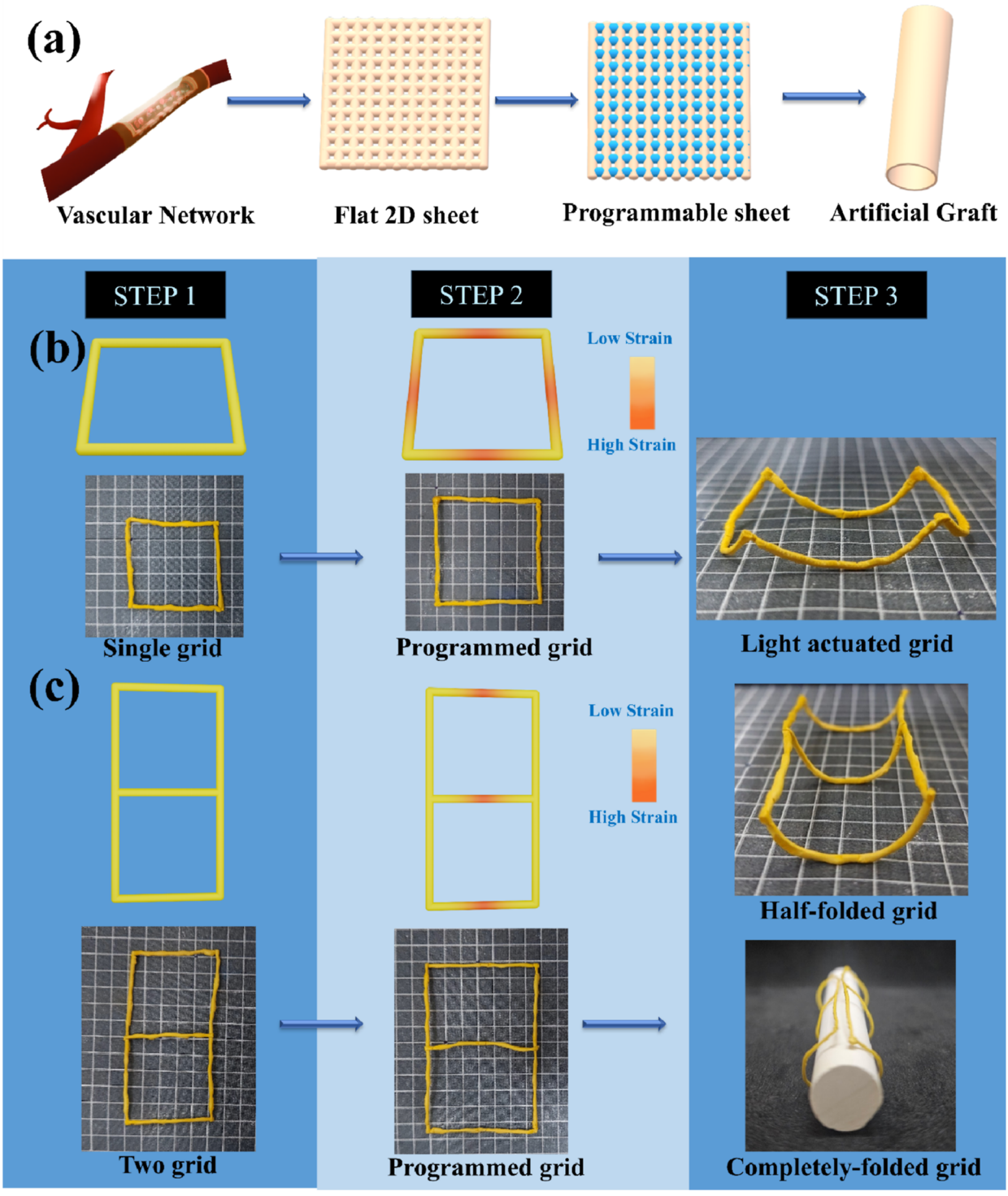

Figure 7. (a) Schematic representation of the steps involved in programming a flat sheet into a 3D vascular graft. Photomechanical deformation of a (b) single- and (c) two-grid structures based on their stress distribution and position of the subjected load.

exhibiting that the deformation is more at the center (based on the strain distribution) than the far end. Similarly, the two-grid construct (Figure 7c) was subjected to load at the center of the three horizontal sides, and the rest of the sides were not prestrained. When irradiated with light, it demonstrates the ability of the grid to deform from flat to (ii) half-curved and (iii) full-curved shapes depending on the bending strain distribution. These responsive constructs were demonstrated as a proof of concept and may have practical application as dynamic scaffold/vascular grafts in tissue engineering to support the growth of cells to regenerate blood vessels or other organs.[49] Individual patients need scaffolds with unique anatomical structures such as blood vessels that vary in diameter and curvature depending upon their location. The fabrication of these complex scaffolds is difficult with the current technology, and hence, these responsive constructs could offer a viable alternative. Our future

https://doi.org/10.1021/acsaenm.5c00225
ACS Appl. Eng. Mater. XXXX, XXX, XXX−XXX

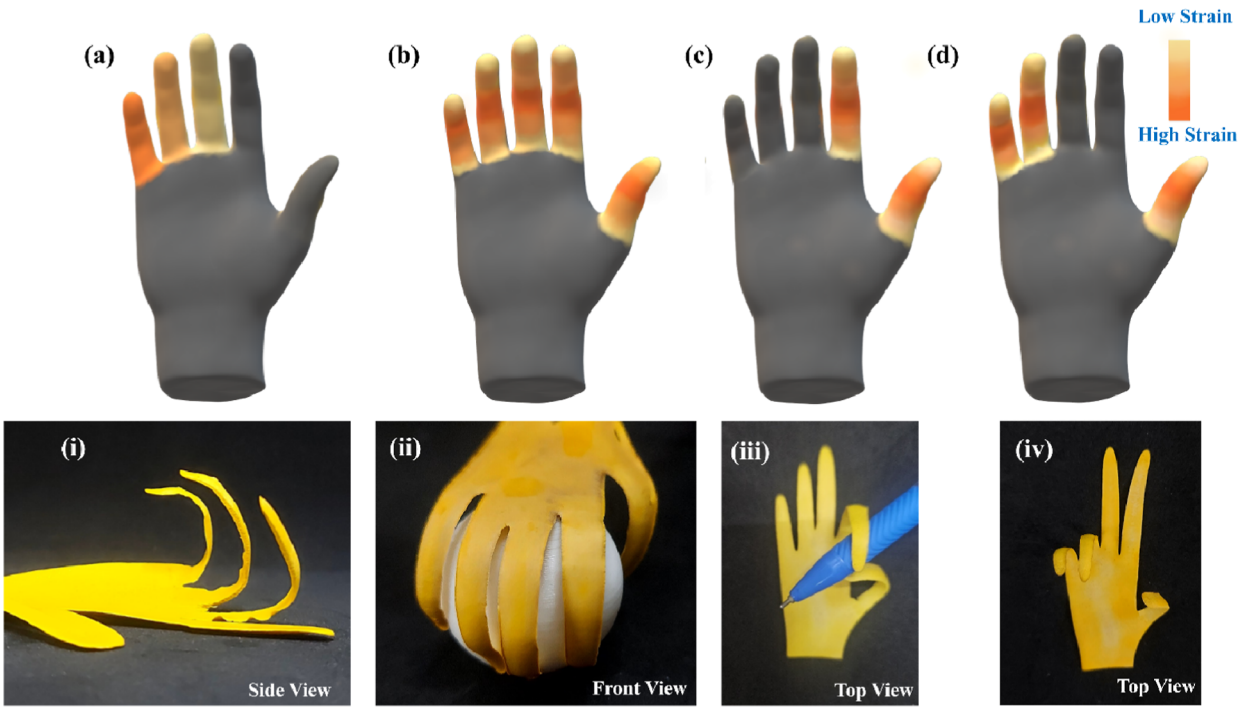

Figure 8. Schematic illustration (a–d) and photoresponsive deformation (i–iv) of the human hand corresponding to the subjected prestrain performing different tasks, i.e., different curvature of each finger, claw hand for grabbing a ball, holding a pen, and victory "V" sign. (The yellow color represents the area undergoing prestrain, and the gray color represents no prestraining).

work envisioned developing photoresponsive structures with a hollow and porous network that can be customized using bending strain. These advanced structures will be designed to undergo a dynamic transformation, enabling them to be used for applications such as wrapping around critical biological structures such as arteries, veins, and other organs. This unique ability would allow them to target drug delivery and nutrient supply, enhancing therapeutic precision. As an example, the SEM image of our hollow and porous TPU is shown in Figure S8, illustrating the foundation of our future work for these innovative applications. Through this approach, we seek to bridge bioengineering with advanced materials by utilizing innovative techniques such as bending strain distribution. This integration allows us to customize responsive systems that address various medical needs effectively.

3.4.2. Soft Robotic Hand. The human hand is an ideal model to demonstrate a controlled and programmable photo-responsive actuation due to its ability to provide synchronous movement and possess a high degree of dexterity. These features enable it to perform different tasks, such as gripping, holding, and manipulating delicate objects with precise coordination and adaptability. In this work, we printed an artificial human hand to program different photomechanical movements or tasks by controlling the bending strain distribution and light irradiation conditions. Figure 8a–d shows the schematic representation of the strain distribution based on the position of the subjected load on different fingers to perform various tasks. Figure 8(i) shows the 3D-printed hand where the three fingers (middle, ring, and pinky) were subjected to different prebending strains before actuation. When the blue light was irradiated onto the fingers, they started to bend toward light and deform with different curvatures depending on the prestrain conditions. This was followed by the demonstration of a claw hand, where we showed that the curvature of the finger can further be tuned by changing the irradiation point to grab a ball (Figure 8(ii)). When the light was irradiated on the distal interphalangeal finger line, sharp bending was observed, exhibiting the ability of light to tune the curvature even when the strain was constant. Therefore, changing the light irradiation point may help in tuning the curvature. In the subsequent experiment, the holding of a pen was demonstrated by subjecting the index finger and thumb to the prebending strain (Figure 8(iii)). The pen was held in the air, and the fabricated hand was brought closer to actuate. After irradiation with light, only the thumb and index finger started to actuate to hold the pen; the rest of the fingers remained in their original position. We also demonstrated the victory "V" sign by subjecting the thumb, ring, and pinky finger to the prebending strain (Figure 8(iv)). These results indicate that the artificial human hand based on light irradiation points and tunable prestraining strategies has a huge potential in soft robotics and biomimicry.

The aforementioned examples demonstrate the enormous potential of the fabricated TPU-BIFA samples. The parametric study on tuning the curvature based on the strain distribution, particularly along the length, helps attain different complex shapes. The versatile strategies, i.e., DIW via the LLPS principle and bending strain demonstrated in this work, could pave the way for numerous future applications such as personalized healthcare, soft robotics, biomimicry, etc. However, this approach is limited to reliance on point-based light exposure rather than global actuation. While point-based actuation allows for more localized and precise control, it increases operational complexity and limits actuation precision. To enhance the actuation reproducibility and ease of control over the system, our future research will consider methods where the filaments can be programmed via bending strain, and the entire structure will be exposed to global light actuation to take a desired shape. Another aspect of improvement would be to utilize the LLPS

https://doi.org/10.1021/acsaenm.5c00225
ACS Appl. Eng. Mater. XXXX, XXX, XXX–XXX

principle for printing more complex structures, taking it a step closer to real-world applications.

4. CONCLUSIONS

In this contribution, we present a prebending strain strategy to program 4D printed structures fabricated using a liquid−liquid phase separation (LLPS) mechanism for controlled and programmable photomechanical deformation. LLPS strategy exhibits immediate curing of the TPU-BIFA composite to enable the printing of complex structures. BIFA dye was introduced into TPU to endow blue light-responsive functionality. Compared with the traditional uniaxial prestraining, we demonstrated bending strain to program localized photomechanical deformation by varying various parameters such as (i) strain magnitude, (ii) concentration of photoresponsive dye, (iii) position of load, (iv) filament diameter, (v) intensity of light, and (vi) point of light irradiation. Building upon comprehending the above-mentioned parameters, we designed 3D printed grid-like and human hand-like models to show different complex geometries from flat to curved shapes and perform various tasks in response to light. We believe that this work could play a pivotal role in the development of a soft actuator for biomimetics and personalized healthcare. In the future, we aim to use this concept to develop tailored photoresponsive vascular grafts or implants required for the specific needs of individual patients.

■ ASSOCIATED CONTENT

Supporting Information

The Supporting Information is available free of charge at https://pubs.acs.org/doi/10.1021/acsaenm.5c00225.

Cross-sectional SEM images of porous TPU-BIFA, TGA curves of TPU, BIFA, and its composite, XRD of the TPU-BIFA before and after bending strain, UV−vis spectra of BIFA dye solution in DMF irradiated with blue LED light (455 nm) for different periods of time, IR thermal images of a filament irradiated with a blue light (455 nm) at different light intensities, schematic representation of two loads subjected at different positions and comparison of light-induced curvature of the TPU-BIFA filaments when subjected to two-point loads, i.e., symmetric and asymmetric loads at different positions, digital images of the curvature change at each point by varying the number of light irradiation points, cross-sectional SEM images of porous and hollow TPU (PDF)

Embedded printing process of a grid structure (MP4)

Photomechanical response of the filament (MP4)

Omnidirectional photoresponsive actuation to form "S" shape (MP4)

■ AUTHOR INFORMATION

Corresponding Author

Pijush Ghosh − *Department of Applied Mechanics and Biomedical Engineering, Indian Institute of Technology Madras, Chennai 600036, India; Center for Soft and Biological Matter, Indian Institute of Technology Madras, Chennai 600036, India;* orcid.org/0000-0002-6077-6498; Email: pijush@iitm.ac.in

Authors

Anas Saifi − *Department of Applied Mechanics and Biomedical Engineering, Indian Institute of Technology Madras, Chennai 600036, India; Center for Soft and Biological Matter, Indian Institute of Technology Madras, Chennai 600036, India*

Smruti Parimita − *Manufacturing Engineering Section, Department of Mechanical Engineering, Indian Institute of Technology Madras, Chennai 600036, India*

Amit Kumar − *Department of Applied Mechanics and Biomedical Engineering, Indian Institute of Technology Madras, Chennai 600036, India;* orcid.org/0000-0002-9935-3775

Complete contact information is available at: https://pubs.acs.org/10.1021/acsaenm.5c00225

Author Contributions

Anas Saifi: Conceptualization, Methodology, Investigation, Data curation, Validation, Writing−review and editing, Writing—original draft. **Smruti Parimita:** Investigation, Data curation, Validation, Writing−review and editing. **Amit Kumar:** Data curation, Validation, Writing−review and editing. **Pijush Ghosh:** Conceptualization, Resources, Writing−review and editing, Supervision.

Notes

The authors declare no competing financial interest.

■ ACKNOWLEDGMENTS

The authors would like to acknowledge the financial support from the Science and Engineering Research Board (SERB), Government of India, for supporting this work (Project No. CRG/2022/007942).

■ REFERENCES

(1) Bodaghi, M.; Wang, L.; Zhang, F.; Liu, Y.; Leng, J.; Xing, R.; Dickey, M. D.; Vanaei, S.; Elahinia, M.; Hoa, S. V.; Zhang, D.; et al. 4D Printing Roadmap. *Smart Mater. Struct.* **2024**, *33* (11), 113501.

(2) Li, M.; Pal, A.; Aghakhani, A.; Pena-Francesch, A.; Sitti, M. Soft Actuators for Real-World Applications. *Nat. Rev. Mater.* **2022**, *7* (3), 235−249.

(3) Janbaz, S.; Hedayati, R.; Zadpoor, A. A. Programming the Shape-Shifting of Flat Soft Matter: From Self-Rolling/Self-Twisting Materials to Self-Folding Origami. *Mater. Horiz.* **2016**, *3* (6), 536−547.

(4) Fan, X.; Chung, J. Y.; Lim, Y. X.; Li, Z.; Loh, X. J. Review of Adaptive Programmable Materials and Their Bioapplications. *ACS Appl. Mater. Interfaces* **2016**, *8* (49), 33351−33370.

(5) Xie, F.; Hou, X.; Sheng, T.; Li, R.; Deng, Z. Harnessing Pattern Transformation of Honeycomb Structures for Soft Actuators Design. *Composites, Part B* **2025**, *295*, 112217.

(6) Liu, H.; Wang, F.; Wu, W.; Dong, X.; Sang, L. 4D Printing of Mechanically Robust PLA/TPU/Fe3O4Magneto-Responsive Shape Memory Polymers for Smart Structures. *Composites, Part B* **2023**, *248*, 110382.

(7) Boley, J. W.; van Rees, W. M.; Lissandrello, C.; Horenstein, M. N.; Truby, R. L.; Kotikian, A.; Lewis, J. A.; Mahadevan, L. Shape-Shifting Structured Lattices via Multimaterial 4D Printing. *Proc. Natl. Acad. Sci. U.S.A.* **2019**, *116* (42), 20856−20862.

(8) Sobinov, A. R.; Bensmaia, S. J. The Neural Mechanisms of Manual Dexterity. *Nat. Rev. Neurosci.* **2021**, *22* (12), 741−757.

(9) Gu, M.; Echtermeyer, T. J. A Graphene-Mica-Based Photo-Thermal Actuator for Small-Scale Soft Robots. *Small* **2024**, *20* (28), 2311001.

(10) O'Connor, C.; Brady, E.; Zheng, Y.; Moore, E.; Stevens, K. R. Engineering the Multiscale Complexity of Vascular Networks. *Nat. Rev. Mater.* **2022**, *7* (9), 702−716.

(11) Goodarzi Hosseinabadi, H.; Biswas, A.; Bhusal, A.; Yousefinejad, A.; Lall, A.; Zimmermann, W.-H.; Miri, A. K.; Ionov, L. 4D-Printable Photocrosslinkable Polyurethane-Based Inks for Tissue Scaffold and Actuator Applications. *Small* **2024**, *20* (6), 2306387.
(12) Pan, B.; Park, S. M.; Ying, W. B.; Yoon, D. K.; Lee, K. J. Azo-Functionalized Thermoplastic Polyurethane for Light-Driven Shape Memory Materials. *Macromol. Rapid Commun.* **2023**, *44* (3), 2200650.
(13) Zhang, H.; Huang, S.; Qian, Z.; Zhang, Y.; Sheng, J.; Zhang, J.; Agyenim-Boateng, E.; Gao, Y.; Lu, J. Tunable Deformation Behavior of 4D Printed Shape Memory Polymers with Embedded Pre-Stretched Elastomers. *Chem. Eng. J.* **2024**, *492*, 152187.
(14) Li, S.; Tu, Y.; Bai, H.; Hibi, Y.; Wiesner, L. W.; Pan, W.; Wang, K.; Giannelis, E. P.; Shepherd, R. F. Simple Synthesis of Elastomeric Photomechanical Switches That Self-Heal. *Macromol. Rapid Commun.* **2019**, *40* (4), 1800815.
(15) Jayoti, D.; Peeketi, A. R.; Kumbhar, P. Y.; Swaminathan, N.; Annabattula, R. K. Geometry Controlled Oscillations in Liquid Crystal Polymer Films Triggered by Thermal Feedback. *ACS Appl. Mater. Interfaces* **2023**, *15* (14), 18362−18371.
(16) Kumar, V.; Satapathy, D. K. Responsive Soft Actuator: Harnessing Multi-Vapor, Light, and Magnetic Field Stimuli. *Soft Matter* **2024**, *20* (27), 5435−5446.
(17) Ceamanos, L.; Mulder, D. J.; Kahveci, Z.; López-Valdeolivas, M.; Schenning, A. P. H. J.; Sánchez-Somolinos, C. Photomechanical Response under Physiological Conditions of Azobenzene-Containing 4D-Printed Liquid Crystal Elastomer Actuators. *J. Mater. Chem. B* **2023**, *11* (18), 4083−4094.
(18) Saed, M. O.; Ambulo, C. P.; Kim, H.; De, R.; Raval, V.; Searles, K.; Siddiqui, D. A.; Cue, J. M. O.; Stefan, M. C.; Shankar, M. R.; Ware, T. H. Molecularly-Engineered, 4D-Printed Liquid Crystal Elastomer Actuators. *Adv. Funct. Mater.* **2019**, *29* (3), 1806412.
(19) Parimita, S.; Kumar, A.; Krishnaswamy, H.; Ghosh, P. Solvent Triggered Shape Morphism of 4D Printed Hydrogels. *J. Manuf. Process.* **2023**, *85*, 875−884.
(20) Shi, G.; Tian, M.; Chen, Y.; Zhong, L.; Zhang, W.; Chen, Z.; Sun, S.; Xia, R.; Iwuoha, E. I.; Peng, X. Nanocellulose-Based Ink for Vertically 3D Printing Micro-Architectures with High-Resolution. *Adv. Funct. Mater.* **2024**, *34* (17), 2311060.
(21) Kumar, A.; Parimita, S.; Kiran, K.; Mahapatra, N. R.; Ghosh, P. Superhydrophobic Asymmetric PH-Responsive Soft Actuators: Implications for the Development of Anti-Fouling Medical Devices. *Chem. Eng. J.* **2024**, *497*, 154772.
(22) Rivera-Tarazona, L. K.; Shukla, T.; Singh, K. A.; Gaharwar, A. K.; Campbell, Z. T.; Ware, T. H. 4D Printing of Engineered Living Materials. *Adv. Funct. Mater.* **2022**, *32* (4), 2106843.
(23) Reynolds, D. S.; de Lázaro, I.; Blache, M. L.; Liu, Y.; Jeffreys, N. C.; Doolittle, R. M.; Grandidier, E.; Olszewski, J.; Dacus, M. T.; Mooney, D. J.; Lewis, J. A. Microporogen-Structured Collagen Matrices for Embedded Bioprinting of Tumor Models for Immuno-Oncology. *Adv. Mater.* **2023**, *35* (33), 2210748.
(24) Mondal, D.; Willett, T. L. Dispersion Strategy Improves the Mechanical Properties of 3D-Printed Biopolymer Nanocomposite. *Composites, Part B* **2024**, *283*, 111680.
(25) Hausladen, M. M.; Gorbea, G. D.; Francis, L. F.; Ellison, C. J. UV-Assisted Direct Ink Writing of Dual-Cure Polyurethanes. *ACS Appl. Polym. Mater.* **2024**, *6* (4), 2253−2265.
(26) Li, H.; Xia, Y.; Guo, R.; Wang, H.; Wang, X.; Yang, Z.; Zhao, Y.; Li, J.; Wang, C.; Huan, S. Direct-Ink-Writable Nanocellulose Ternary Hydrogels via One-Pot Gelation with Alginate and Calcium Montmorillonite. *Carbohydr. Polym.* **2024**, *344*, 122494.
(27) Tang, L. Liquid Phase Separation. *Nat. Methods* **2019**, *16* (1), 18.
(28) Deng, X.; Yang, F.; Ma, J.; Li, Y.; Dang, J.; Ouyang, M. Ternary Phase Field Model and Characterization of Water/NMP/Polysulfone Membrane Prepared by Non-Solvent Induced Phase Separation. *Sep. Purif. Technol.* **2024**, *330*, 125307.
(29) Chen, K.; Li, Z.; Guo, J.; Yang, X.; Guo, B.; Shen, H. A Flexible Capacitive Pressure Sensor Based on Thermoplastic Polyurethane Porous Films by Non-Solvent Induced Phase Separation. *IEEE Sens J.* **2024**, *24* (8), 12217−12224.
(30) Qian, H.-L.; Huang, W.-P.; Fang, Y.; Zou, L.-Y.; Yu, W.-J.; Wang, J.; Ren, K.-F.; Xu, Z.-K.; Ji, J. Fabrication of "Spongy Skin" on Diversified Materials Based on Surface Swelling Non-Solvent-Induced Phase Separation. *ACS Appl. Mater. Interfaces* **2021**, *13* (48), 57000−57008.
(31) Santra, A.; Prakash, R.; Maity, S.; Nilawar, S.; Chatterjee, K.; Maiti, P. Core−Shell Structure of Photopolymer-Grafted Polyurethane as a Controlled Drug Delivery Vehicle for Biomedical Application. *ACS Appl. Mater. Interfaces* **2024**, *16* (14), 17193−17207.
(32) Bhattacharya, S.; Hailstone, R.; Lewis, C. L. Thermoplastic Blend Exhibiting Shape Memory-Assisted Self-Healing Functionality. *ACS Appl. Mater. Interfaces* **2020**, *12* (41), 46733−46742.
(33) Xu, B.; Zhu, C.; Qin, L.; Wei, J.; Yu, Y. Light-Directed Liquid Manipulation in Flexible Bilayer Microtubes. *Small* **2019**, *15* (24), 1901847.
(34) Jiang, H. Y.; Kelch, S.; Lendlein, A. Polymers Move in Response to Light. *Adv. Mater.* **2006**, *18* (11), 1471−1475.
(35) Hu, J.; Feng, Z.; Xu, X.; Gao, W.; Ning, N.; Yu, B.; Zhang, L.; Tian, M. UV Reconfigurable Shape Memory Polyurethane with a High Recovery Ratio under Large Deformation. *Ind. Eng. Chem. Res.* **2021**, *60* (5), 2144−2153.
(36) Xie, H.; He, M.; Deng, X.-Y.; Du, L.; Fan, C.-J.; Yang, K.-K.; Wang, Y.-Z. Design of Poly(l-Lactide)−Poly(Ethylene Glycol) Copolymer with Light-Induced Shape-Memory Effect Triggered by Pendant Anthracene Groups. *ACS Appl. Mater. Interfaces* **2016**, *8* (14), 9431−9439.
(37) Zheng, Y.; Huang, H.; Wang, Y.; Zhu, J.; Yu, J.; Hu, Z. Poly (Vinyl Alcohol) Based Gradient Cross-Linked and Reprogrammable Humidity-Responsive Actuators. *Sens. Actuators, B* **2021**, *349*, 130735.
(38) Gastaldi, M.; Spiegel, C. A.; Vazquez-Martel, C.; Barolo, C.; Roppolo, I.; Blasco, E. 4D Printing of Light Activated Shape Memory Polymers with Organic Dyes. *Mol. Syst. Des Eng.* **2023**, *8* (3), 323−329.
(39) Saifi, A.; Negi, C.; Singh, A. P.; Kumar, K. Visible Light Responsive Soft Actuator Based on PVA-DR1. *ChemistrySelect* **2023**, *8* (39), No. e202301628.
(40) Saifi, A.; Negi, C.; Kumar, K. Visible Light Responsive Soft Actuator Based on Functional Anthracene Dye. *Eur. Polym. J.* **2022**, *171*, 111176.
(41) Wu, L.; Huang, X.; Wang, M.; Chen, J.; Chang, J.; Zhang, H.; Zhang, X.; Conn, A.; Rossiter, J.; Birchall, M.; Song, W. Tunable Light-Responsive Polyurethane-Urea Elastomer Driven by Photochemical and Photothermal Coupling Mechanism. *ACS Appl. Mater. Interfaces* **2024**, *16* (15), 19480−19495.
(42) Shi, X.; Zhang, K.; Chen, J.; Qian, H.; Huang, Y.; Jiang, B. Octopi Tentacles-Inspired Architecture Enables Self-Healing Conductive Rapid-Photo-Responsive Materials for Soft Multifunctional Actuators. *Adv. Funct. Mater.* **2024**, *34* (6), 2311567.
(43) Jiang, Z.; Tan, M. L.; Taheri, M.; Yan, Q.; Tsuzuki, T.; Gardiner, M. G.; Diggle, B.; Connal, L. A. Strong, Self-Healable, and Recyclable Visible-Light-Responsive Hydrogel Actuators. *Angew. Chem., Int. Ed.* **2020**, *59* (18), 7049.
(44) Zheng, Y.; Huang, H.; Yu, J.; Hu, Z.; Wang, Y. Highly Stretchable and Strong Poly (Vinyl Alcohol)-Based Hydrogel for Reprogrammable Actuator Applications. *Chem. Eng. J.* **2023**, *454*, 140054.
(45) Bi, X.; Song, K.; Zhang, Z.; Lin, T.; Pan, Y.-T.; Fu, W.; Song, P.; He, J.; Yang, R. Joint Exfoliation of MXene by Dimensional Mismatched SiC/ZIF-67 Toward Multifunctional Flame Retardant Thermoplastic Polyurethane. *Small* **2024**, *20* (43), 2403375.
(46) Ren, L.; Wang, Z.; Ren, L.; Liu, Q.; Li, W.; Song, Z.; Li, B.; Wu, Q.; Zhou, X. 4D Printing of Shape Memory Composites with Remotely Controllable Local Deformation. *Mater. Today Chem.* **2023**, *29*, 101470.
(47) Zolfagharian, A.; Bodaghi, M. Robotic materials 4D printing. *Smart Materials in Additive Manufacturing, Volume 3:4D-Printed Robotic Materials, Sensors, and Actuators* **2024**, 1−11.
(48) Afzali Naniz, M.; Askari, M.; Zolfagharian, A.; Afzali Naniz, M.; Bodaghi, M. 4D printing: a cutting-edge platform for biomedical applications. *Biomed. Mater.* **2022**, *17* (6), 062001.

https://doi.org/10.1021/acsaenm.5c00225
ACS Appl. Eng. Mater. XXXX, XXX, XXX−XXX

(49) Diba, M.; Koons, G. L.; Bedell, M. L.; Mikos, A. G. 3D Printed Colloidal Biomaterials Based on Photo-Reactive Gelatin Nanoparticles. *Biomaterials* **2021**, *274*, 120871.

https://doi.org/10.1021/acsaenm.5c00225
ACS Appl. Eng. Mater. XXXX, XXX, XXX−XXX